JGR Biogeosciences

RESEARCH ARTICLE
10.1029/2024JG008080

Navigating Greenhouse Gas Emission Unknowns: A Hydroacoustic Examination of Mediterranean Climate Reservoirs

R. H. Thirkill[1,2], Cintia L. Ramón[3], Holly J. Oldroyd[1,2], Mark Seelos[4], Francisco J. Rueda[3], and Alexander L. Forrest[1,2]

[1]Department of Civil and Environmental Engineering, University of California Davis, California, CA, USA, [2]Tahoe Environmental Research Center, University of California Davis, California, CA, USA, [3]Department of Civil and Environmental Engineering and Water Institute, University of Granada, Granada, Spain, [4]Santa Clara Valley Water District, San Jose, CA, USA

Key Points:

- Hydroacoustic models relying solely on backscatter underestimate gas in shallow, silty sediments and overestimate in larger (>2 mm) ones
- An extension to the current model incorporates gas fraction and sediment type to improve gas predictions
- Bubble plume mapping reveals ebullition hotspots are tied to gas storage, bottom temperature, dissolved oxygen, and sediment type

Supporting Information:

Supporting Information may be found in the online version of this article.

Correspondence to:

R. H. Thirkill,
rthirkill@ucdavis.edu

Citation:

Thirkill, R. H., Ramón, C. L., Oldroyd, H. J., Seelos, M., Rueda, F. J., & Forrest, A. L. (2024). Navigating greenhouse gas emission unknowns: A hydroacoustic examination of mediterranean climate reservoirs. *Journal of Geophysical Research: Biogeosciences*, *129*, e2024JG008080. https://doi.org/10.1029/2024JG008080

Received 9 FEB 2024
Accepted 6 NOV 2024

Author Contributions:

Conceptualization: R. H. Thirkill, Holly J. Oldroyd, Alexander L. Forrest
Data curation: R. H. Thirkill
Formal analysis: R. H. Thirkill
Funding acquisition: Cintia L. Ramón, Holly J. Oldroyd, Mark Seelos, Francisco J. Rueda, Alexander L. Forrest
Investigation: R. H. Thirkill, Cintia L. Ramón, Mark Seelos
Methodology: R. H. Thirkill
Project administration: Holly J. Oldroyd, Francisco J. Rueda, Alexander L. Forrest
Resources: Cintia L. Ramón, Mark Seelos, Francisco J. Rueda, Alexander L. Forrest
Visualization: R. H. Thirkill

Abstract Inland aquatic systems, such as reservoirs, contribute substantially to global methane (CH_4) emissions; yet they are among the most uncertain contributors to the total global carbon budget. Reservoirs generate significant amounts of CH_4 within their bottom sediment, where the gas is stored and can easily escape via ebullition. Due to the large spatial and temporal variability associated with ebullition, CH_4 fluxes from these aquatic systems are challenging to quantify. To address these uncertainties, six different water storage reservoirs, with average flux rates ranging between 20 and 678 mg CH_4 m^{-2} d^{-1}, were hydro-acoustically surveyed using a previously established technique to investigate the spatial variability of free gas stored at the sediment surface that could be released as bubbles. Sediment samples and vertical profiles of temperature and dissolved oxygen were also collected to understand their respective influences on sediment gas formation. We found that the established relation used to determine sediment gas storage via the sonar technique, which relied solely on acoustic backscatter (Sv_{max}), tended to underestimate gas storage in shallower, siltier sediment zones and overestimate gas storage in coarser (>2 mm) sediment zones. In response, we introduce an improved model, incorporating gas and sediment type as correction factors for gas attenuation effects on Sv_{max} values. The extended model is able to elucidate patterns within the gas volume data, revealing clearer trends across different sediment types. This research provides valuable data and methodological insights that can enhance the accuracy of greenhouse gas modeling and budget assessments for reservoirs.

Plain Language Summary Inland aquatic systems, like reservoirs, contribute substantially to greenhouse gas emissions, but these systems comprise the most uncertain components of the CH_4 budget. Reservoirs can produce significant amounts of CH_4 in submerged sediments, which escape slowly through diffusion and quickly through bubbling. However, accurately measuring CH_4 emissions from reservoirs is difficult due to significant variability in bubbling patterns over space and time. To better understand these patterns, we surveyed six reservoirs using an established underwater sonar technique to explore the spatial variability of free gas stored in sediments, which could bubble up. We also collected sediment samples and measured dissolved oxygen and temperature at various water depths to study their influence on sediment gas formation. We found that the previously established sonar model used to obtain the amount of gas in the sediments tended to underestimate gas storage in shallower, siltier areas and overestimate it in larger-grained sediment zones. In response, we introduced a refined model that incorporates gas fraction and sediment type to correct for gas attenuation effects on the sonar output. This extended model clarifies gas volume patterns across sediment types. Our study offers valuable data and methodological insights to refine greenhouse gas modeling and budget assessments for reservoirs.

1. Introduction

Current estimates of global greenhouse gas (GHG) emissions from lakes and reservoirs could be equivalent to up to nearly 20% of the global fossil fuel CO_2 emissions, with nearly 75% of the climate impact resulting from methane (DelSontro et al., 2018). Those estimates of global CH_4 emissions from lakes and reservoirs, however, are highly uncertain (Saunois et al., 2020). Moreover, these estimates are based on observations that have been collected in a limited number of lakes and reservoirs (see Barros et al., 2011; Deemer et al., 2016) using sampling designs that typically do not account for the natural variability of CH_4 emissions, both in time and in space.

Writing – original draft: R. H. Thirkill
Writing – review & editing: Cintia L. Ramón, Holly J. Oldroyd, Mark Seelos, Francisco J. Rueda, Alexander L. Forrest

Although recent advancements in sensor technology (Delwiche et al., 2015; Gonzalez-Valencia et al., 2014; Maeck et al., 2014; Podgrajsek et al., 2014), survey designs (Beaulieu et al., 2016; DelSontro et al., 2011; Linkhorst et al., 2020; Wik, Thornton, et al., 2016), and analytical methods (Itoh et al., 2017; Langenegger et al., 2022) have begun to address some of these limitations, there continues to remain significant uncertainty due to the spatial and temporal heterogeneity of methane production and release.

The primary controls over these emissions rest with the GHG gas generation in the interior of anoxic sediments because of the complex microbial metabolism of organic carbon (DelSontro et al., 2016; Duc et al., 2010; Grasset et al., 2018; Moras et al., 2024; West et al., 2016). Dissolved methane can travel across the sediment-water interface, up through the water column to eventually diffuse through the air-water interface into the atmosphere. Conversely, if the net CH_4 production is higher than the diffusive transport from the sediment to the water, porewater dissolved gas concentrations in the sediments will oversaturate and bubbles will form (Langenegger et al., 2019). These bubbles accumulate in the sediments and release into the water column episodically in response to external perturbations that modify the subtle interplay between bubble buoyancy and sediment mechanics (Scandella et al., 2011; Varadharajan & Hemond, 2012). This process of gas transport through rising bubbles (bubbling or ebullition) is likely the most efficient pathway for CH_4 gas to reach the atmosphere in lakes and reservoirs (Bastviken et al., 2010; DelSontro et al., 2015; Wik, Thornton, et al., 2016, Wik, Varner, et al., 2016), since it enables the CH_4 within the bubbles to circumvent CH_4 oxidation by methanotrophs in the water column. In shallow reservoirs, it is the dominant pathway (Bastviken et al., 2004; Rodriguez-Velasco et al., 2024). However, quantifying the dynamics of methane emissions from the bottom sediments, even within the same reservoir (ecosystem scale), is far from complete. This is partly due to the multiplicity of mechanisms, each one with different physical and biogeochemical drivers and hence with different scales of variability controlling the source and fate of CH_4 in the sediments (see Katsnelson et al., 2017; Liu et al., 2020; Marcon et al., 2022, 2023; Uzhansky et al., 2020). A further complication in trying to solve the mass balance for CH_4 at the ecosystem scale is that quantifying ebullitive fluxes remains elusive due to their episodic nature (Varadharajan & Hemond, 2012) and spatial variability. Grinham et al. (2011), for example, reported that 97% of the CH_4 emitted from the surface of a subtropical reservoir was derived from approximately 5% of the reservoir surface area located immediately downstream of the main tributary input. Furthermore, quantifying the amount of gas stored in the bottom sediments of any given lake or reservoir, which serves as the driving force for ebullition (Martinez & Anderson, 2013), remains an open question.

Among direct methods for quantifying gas in sediments, the simplest approach consists of disturbing the sediment surface with an anchor weight at a grid of discrete sites to release bubbles, which are immediately caught with an inverted funnel equipped with a gas container on the top. This approach, though straightforward, is invasive and provides only point estimates (i.e., of limited spatial extent) of gas content. A more recent alternative consists of the use of hydroacoustic technology. Gas bubbles are strong scatterers of acoustic energy, given the large density difference between water or sediments and the bubbles. Hence, bubbles can be detected using scientific echo sounders. This hydroacoustic technology has a large potential for the noninvasive survey of the spatial heterogeneity of total gas storage in the sediments at ecosystem scales (Martinez & Anderson, 2013). Based on samples collected in two lakes and one reservoir in Southern California, Anderson and Martinez (2015) developed an empirical equation (AM2015 hereafter) to estimate the gas volume contained in the sediment per unit area from the maximum backscatter strength (Sv_{max}) at a frequency of 201 kHz. In developing their predictive equations, they discarded sediment samples containing <60% water content and <2% organic carbon. Hence, the application of AM2015 could be limited and should be evaluated prior to being used in other systems. Still, it has been used without further validation (e.g., Marcon et al., 2022), or if validated (e.g., Marcon et al., 2023), the acoustic collection parameters differed from those of Anderson and Martinez (2015). These collection parameters could affect the value of Sv_{max}, and thus, a robust validation of the AM2015 model is still necessary.

In contrast, recent studies have delved into alternative acoustic techniques for gas quantification. For instance, Katsnelson et al. (2022, 2017), and Uzhansky et al. (2020) applied an inverse geoacoustic technique to derive the speed of sound in the sediment to estimate its gas storage and therefore spatial variability. However, this technique depends on the nonlinear relationship between sound speed and gas content which leads to a substantial increase in error of the gas estimates at low sound speeds (Katsnelson et al., 2017, 2022; Uzhansky et al., 2020). Furthermore, the method is numerically intensive and experimentally complex. Alternatively, Liu et al. (2020) employed an acoustic technique similar to the AM2015 model for the same lake but with a two-step procedure. Unlike AM2015, they found no significant correlation between volumetric sediment gas content and acoustic

Table 1
Study Sites and Sonar Settings

	Anderson and Martinez (2015)			This study					
	Southern California, USA			Northern California, USA				Southern Spain	
Name	Elsinore	Hodges	Skinner	Uvas	Chesbro	Stevens Creek	Almaden	Iznájar	Cubillas
Type	Lake	Reservoir	Lake	Reservoir	Reservoir	Reservoir	Reservoir	Reservoir	Reservoir
Mean depth (m)	7.5	7.5	11.2	11	10	11	11	42	4
Max depth (m)	11	35	24	25	24	15	20	85	10
Trophic state	Eutrophic	Eutrophic	Mesotrophic	Mesotrophic	Mesotrophic	Eutrophic	Mesotrophic	Mesotrophic	Eutrophic
Echo sounder	BioSonics DTX-200			BioSonics DTX-200					
Frequency (kHz)	201			201					
Pulse duration, τ (ms)	0.4			0.4					

parameters. Instead, they identified two distinct correlations: first, between the in situ dissolved porewater CH_4 concentration (DCH_4) and the acoustic backscatter strength during the second phase of the echo and second, between the in situ sediment gas content and DCH_4 (Liu et al., 2020). As a result, the existing AM2015 model continues to be the simplest, most direct method to quantify the magnitude and spatial variability of gas storage in bottom sediments at the ecosystem scale. However, uncertainties concerning its application across diverse systems persist (i.e., sediments with <60% water content and <2% organic carbon).

In response, hydroacoustic surveys were conducted across six different freshwater reservoir sites in Northern California and southern Spain with similar Mediterranean climates. Temperature and dissolved oxygen (DO) vertical profiles were collected concurrently to sediment gas volume and grab samples at various grid points. Our key objectives are to (a) assess the functionality of the existing AM2015 model in new reservoir systems, (b) expand its applicability to a broader range of sediments and reservoir conditions, and (c) model the spatial distribution of gas content in one reservoir using the new expanded model to enhance our understanding of where gas storage and ebullition hotspots are likely to emerge.

2. Methods

To develop a systematic approach for an extensive investigation of the GHG production and related parameters in a reservoir, hydroacoustic methods were combined with physiochemical sediment variables and sediment gas measurements (see Figure S1 in Supporting Information S1 for methodological approach). All data collected were used to assess and compare the AM2015 model to the newly expanded model, but only the survey conducted at Uvas Reservoir in summer 2021 was used to explore the spatial variability of gas storage and ebullition hotspots.

2.1. Study Reservoirs

Measurements were made at 4 reservoirs located within the Santa Clara County Valley Water District, in Northern California, USA, and two Spanish reservoirs located in the country's southern region of Andalusia. Quarterly hydroacoustic measurements were collected at Uvas, Chesbro, and Stevens Creek Reservoirs between fall 2020 and fall 2022. Additional surveys were conducted at Almaden (USA), Cubillas, and Iznájar Reservoirs (Spain) to expand the data set in 2022. A second acoustic experiment was conducted on Cubillas in fall 2023. Unlike Uvas, Stevens Creek, and Chesbro, Almaden has a hypolimnetic oxygenation system installed in the deepest region of the reservoir, which could limit gas production in the reservoir sediments; this system was operating during the survey. Cubillas and Iznájar, located in Southern Spain, were included to determine if similar trends occur in different parts of the world with similar climatic conditions (details on GHG emissions from these two reservoirs can be found in León-Palmero et al., 2020). Each system exhibits typical characteristics for Mediterranean climate reservoirs, meaning they experience large fluctuations in both surface area and volume on a yearly basis due to seasonal hydrologic changes and demands. The reservoirs were built between the mid-1930s and 1960s, and they are all mesotrophic or eutrophic monomictic reservoirs. Basic details on the study reservoirs are presented in Table 1. All the reservoirs receive inflow from local precipitation during the wet season (November to April) and little to no precipitation during the dry season.

Table 2
Sediment Parameters From Grab Samples Taken From All Study Reservoirs

	n	Mean	Max	Min	SD	CV
Depth (m)	141	9.7	27.0	1.2	6.2	0.6
H_2O (%)	70	60.3	74.1	18.0	10.8	0.2
LOI (%)	64	8.4	12.2	2.7	1.7	0.2
OrgC (%)	76	2.4	5.2	0.3	0.9	0.4
Sand (volume %)	77	13.8	95.4	0.0	23.9	1.7
Silt (volume %)	77	74.5	91.9	4.2	19.6	0.3
Clay (volume %)	77	11.7	21.5	0.4	6.1	0.5

Note. *n*, number of samples; SD, standard deviation; and CV, coefficient of variation.

2.2. Hydroacoustic Measurements

Hydroacoustic measurements were conducted, as in AM2015. A 201-kHz transducer was connected to a BioSonics DTX-200 echo sounder surface unit (Seattle, WA, USA) and a Garmin real-time differential GPS receiver. Data were collected on a Dell laptop running BioSonics Visual Acquisition 6 software. For all surveys, the ping rate on the BioSonics was set to five pings per second, with a 0.4-ms pulse duration (τ). The transducer was calibrated in the field once a year using a tungsten carbide calibration sphere suspended about 5 m below the transducer's face. The water column and bottom sediments were scanned with the echo sounder while the vessel was driving along transect lines at speeds around 1.5 m s^{-1}. All depths were sampled except very shallow regions (<1.6 m) where no adequate echo signals could be received (beam angle = 6.6°, transducer depth = 0.5 m, and nearfield zone = 1.6 m).

During sediment sampling, the boat was fixed to one position by deploying an anchor. To minimize disturbing the sediments directly below the sonar head, the anchor was deployed on the opposite side of the vessel from the echo sounder. In cases of high winds, two anchors were used to prevent the vessel from drifting. Latitude and longitude data from the echo sounder's GPS were used to assess any drift during sediment sampling. Samples showing a drift distance greater than the footprint of the sonar heads were rejected from any sonar analysis. This occurred in only two cases. Any sediment sample collected below 1.6 m ($n = 2$) were not included in the acoustic statistical analyses but were used in statistical correlations with gas content. Finally, in addition to the reservoir surveys listed above, a second experiment was conducted in fall 2023 on Cubillas Reservoir, using different pulse durations and ping rates along the same transect to determine whether altering these settings impacts the Sv_{max} output. A calibration of the transducer was performed for each pulse width tested, and the corresponding dB offsets were applied prior to data processing.

Bottom typing was performed on acoustic data when there was low gas storage in the sediments (i.e., winter surveys). Fifteen different acoustic attributes of the bottom echo envelope (i.e., E1′, E1, FD, E1′/E1, etc.) were extracted (see Figure S2 in Supporting Information S1) using BioSonics Visual Aquatic software (BioSonics, Seattle, WA, USA (2020)). These features were then normalized and clustered using a Fuzzy C analysis. These steps were performed by the BioSonics Visual Aquatic standard method (BioSonics, Seattle, WA, USA). The output data were then plotted according to the cluster type and spatially compared to the d50 particle size data of the grab samples to identify the distribution of different sediment types within each reservoir. The Fuzzy C analysis was chosen because of its ability to assign degrees of membership to different categories rather than making strict, binary decisions. This allows for a more flexible and nuanced analysis, especially when dealing with complex information like sediment type. Sv_{max} was directly extracted from the raw echograms.

2.3. Sediment Sampling

Sediment properties (including gas volume, loss on ignition (LOI), and sediment type, see Table 2 for a complete list) were estimated from samples collected at 3–6 discrete locations (Figure S16 in Supporting Information S1) in each reservoir along the boat trajectories. At each location, stationary echo sounder measurements were conducted for 1–5 min. After these measurements, various sediment sampling measurements were made within the footprint of the echo sounder beam. The volume of gas present in the bottom sediments was measured by lowering

a cylindrical weight with a known cross-sectional area (0.0045 m^2) into the sediments and capturing the released gas into an inverted cylinder initially filled with water. The amount of gas displaced from the sediments was then measured by bringing the sampler to the water surface and corrected for local hydrostatic pressure at depth using the ideal gas law. Sediment gas fraction (n_g) was calculated using the values listed in the SI (Text S3, Table S5 in Supporting Information S1) and the following equations:

$$n_g = \frac{V_g}{V_s} \quad (1)$$

$$V_s = A_w z \quad (2)$$

where V_g is the measured volume of displaced gas (corrected for hydrostatic pressure), V_s is the sediment volume depressed by the sampling chamber weight, A_w is the cross-sectional surface area of the chamber weight, and z is the penetration depth of the chamber weight. A detailed description of the gas sampling chamber and corresponding measurements (A_w, V_s, and z) is provided in the Supporting Information (Text S2 in Supporting Information S1). If the total volume of measured sediment gas was greater than 25 mL, replicate samples were collected for gas composition analysis into evacuated 12 mL screw-top soda glass vials capped with a silicone-coated Teflon septum stacked on top of a chlorobutyl septum (Labco Ltd, UK). Nitrous oxide (N_2O), carbon dioxide (CO_2), and CH_4 were analyzed on a Shimadzu gas chromatograph-14 (GC) system equipped with an electron capture detector for N_2O, thermal conductivity detector for CO_2, and a flame ionization detector (FID temperature = 250°C) for CH_4 with helium as the carrier gas. These detectors have a repeatability of <2% for standards 600 ppm CO_2, 1 ppm N_2O, and 5 ppm CH_4. For the remainder of the sediment properties (i.e., organic matter content, etc.), sediment samples were retrieved using an Ekman-Birge grab sampler, homogenized and transferred into a Ziploc™ bag and stored on ice for transport as per Anderson and Martinez (2015). Though other sediment samplers, such as sediment corers, provide more detailed insights into the vertical distribution of water content and particle size, the Ekman Grab sampler has been shown to provide adequate reproducibility (standard deviation < 10%) for capturing surface sediment characteristics, particularly in soft silty and fine sand sediments (Baudo, 2020; Mudroch & MacKnight, 1994). Additionally, Anderson and Martinez (2015) used the Ekman Grab for their sediment sampling, and we chose to remain consistent with their method to enable a direct comparison of results. Once at the lab, the samples were kept at 4°C. Water content was determined gravimetrically by drying 3 replicate aliquots of a known mass of wet sediment to a constant dry weight mass at 105°C overnight and taking the mass difference between the two. Dry sediments were then analyzed for loss on ignition (LOI) using a muffle furnace set to 550°C for 4 hr, giving a rough estimate of the organic matter content. In addition to the LOI, the organic carbon content (OrgC) in the sediments was measured by the University of California, Davis Analytical laboratory from replicate sediment samples (n = 3) pretreated with phosphoric acid to remove the inorganic carbon, rinsed with deionized water and dried at 105°C overnight. Finally, samples were sieved to remove particles >2 mm and noted. The remaining material was then measured using a Beckman Coulter LS230 laser granulometer to get particle size distributions for sizes ranging from 0.04 to 2,000 μm.

2.4. Water Quality Measurements

At each sampling site, temperature (ºC), water depth (m), and dissolved oxygen (DO in mg/L) profiles were collected using a Hydrolab DS5 sonde. Measurements were taken every quarter meter for the first meter of water and then every half meter until the bottom sediments. Vertical profiles of temperature from each sampling location within the same survey date and the reservoir were plotted together to assess the spatial heterogeneity in vertical water temperatures (see Figure S3 in Supporting Information S1). If the temperature differences between profiles at each depth were within 1°C, the data along the deepest vertical profile were used to extrapolate bottom water temperature (BWT) across the entire survey area using the acoustically derived bathymetry. If the temperature differences exceeded 1°C, an average temperature was calculated for each depth.

2.5. Acoustic Models for Predicting the Sediment Gas Content

Two different acoustic regression models were tested for gas content. The first model is the pre-existing Anderson and Martinez (2015) acoustic model (AM2015), where Sv_{max} was correlated with the in situ sediment gas volume measurements (G) as follows:

$$G = e^{(0.327 * Sv_{max} + 3.48)} \quad (3)$$

where G is in L m^{-2} and Sv_{max} is in dB.

An extension of the AM2015 model is proposed here as the second model and uses the sediment gas fraction (n_g) and the sediment type in addition to the measured Sv_{max} to predict sediment gas content. This extended model is referred to as the gas fraction (GFR) model from here on. The development of the GFR model is discussed in Section 3, and further details on how to execute the GFR model are included in the Supplementary Information (Texts S3 and S4 in Supporting Information S1). The model results for gas content predictions were evaluated using the coefficient of determination (R^2), the mean absolute error (MAE), and the root mean squared error (RMSE) between observed and predicted gas content.

2.6. Spatial Mapping of Sediment Gas Content and Bubble Plumes

To assess the sediment gas content against its ebullition potential, we generated two spatial maps of sediment gas content using the AM2015 and GFR models for the summer 2021 survey conducted in Uvas Reservoir (see Text S4 in Supporting Information S1). A spatial grid of 30 m by 30 m was created for the survey track area and mean values of water depth, bottom slope, Sv_{max}, BWT, sediment type, n_g, and gas content were calculated for each grid cell. To reduce the uncertainty of parameters derived from the acoustic measurements, we excluded grid cells where the grazing angle of the sound wave could introduce artifacts into the signal. This includes all grid cells with an average bottom slope larger than 10° (Fonseca et al., 2002; Huang et al., 2018; Marcon et al., 2022; Sternlicht & de Moustier, 2003). Bubble plumes (not flux) were identified visually on the echograms, and their geographic location was tagged (see Figure S4 in Supporting Information S1). The sediment gas content data were then grouped into 1-m water depth bins, and the average gas content for each bin was calculated. These averages were then quantitively correlated with the total number of observed bubble plumes in each bin.

3. GFR Model Development

Gas bubbles are a common occurrence in fine-grained, organic-rich freshwater sediments (Martinez & Anderson, 2013; Wilkens & Richardson, 1998). Even in small quantities, these bubbles can significantly influence the geoacoustic properties of reservoir bottom sediments, altering the propagation of acoustic waves (Anderson et al., 1998; Lyons et al., 1996; Wilkens & Richardson, 1998). Typically, Sv_{max} increases with gas content, but the rate of change is much lower in shallow sediments than those lying below deepwater columns, due to bubble effects and the sediment type. Given these complexities, it is recommended that acoustic models account for both bubble effects and sediment characteristics when modeling gas content (Fonseca et al., 2002; Wilkens & Richardson, 1998). The AM2015 model, however, does not address these factors, leading us to develop the gas fraction (GFR) model to overcome these limitations.

Past research suggests that the difference in Sv_{max} between shallow versus deep highly gaseous sediments can either be due to (1) the decrease of sediment sound speed in the presence of gas below resonance or (2) an increase in sound attenuation in the presence of gas above resonance and with high sediment gas fractions (Anderson & Hampton, 1980a, 1980b; Fonseca et al., 2002; Tóth et al., 2015; Wilkens & Richardson, 1998). The impact of either phenomenon depends on the water depth and bubble size, but most importantly on the ratio between the bubble resonance frequency f_0 and the sonar acoustic frequency f (Anderson & Hampton, 1980a, 1980b; Fonseca et al., 2002; Tóth et al., 2015; Wilkens & Richardson, 1998). Furthermore, the sediments for which f_0 effects are most significant are the fine-grained silts and clays (Anderson & Hampton, 1980a, 1980b). The f_0 of a bubble in the sediment is related to the resonance of that same bubble in the water modified by the elastic properties of the surrounding solid (the sediment) and can be calculated as follows (Anderson & Hampton, 1980a, 1980b):

$$f_0 = \frac{\left(\frac{3\gamma P_0}{A\rho_s} + \frac{4G}{\rho_s}\right)^{0.5}}{2\pi r_0} \quad (4)$$

Here γ is the ratio of specific heats of gas, P_0 is the ambient hydrostatic pressure, ρ_s is the wet density of the sediment, G is the real part of the sediment dynamic shear modulus, r_0 is the bubble radius, and A is the polytropic coefficient.

Sound speed in gaseous sediments (c) is similar to that in bubble-free sediments (c_o) for $f > f_0$, while for $f < f_0$, in turn, sound speed significantly decreases as the sonar frequency is reduced (Anderson & Hampton, 1980a, 1980b; Wilkens & Richardson, 1998). On the other hand, attenuation is highest at f_0, decreasing rapidly at f_0 above and below bubble resonance. In gaseous sediments, containing a mixture of bubble sizes, the frequency-dependent sound speed, its attenuation, and, hence, the acoustic return are a summation of the combined effects of various bubble sizes in the population (Boyle & Chotiros, 1995; Tóth et al., 2015). Using Equation 4, we calculated our resonance bubble radius to be $r_o = 0.44$ mm ($f_0 = 202$ kHz). This means that for bubbles with a radius of $r_0 \leq 0.44$ mm, the speed of sound in the sediments is significantly less than the speed of sound in the overlaying water. However, according to the literature, most bubbles in soft sediments have $r_0 = 0.5$–5 mm (See Text S3, Table S3 in Supporting Information S1) with higher numbers for smaller bubbles (Anderson et al., 1998). This range is above our resonance threshold ($r_0 = 0.44$ mm); therefore, we assume that the speed of sound in our sediments is the same as the speed of sound in the overlaying water (~1,500 m/s) leading to the conclusion that sediment attenuation is likely the culprit for the discrepancy in the data.

We calculated the sediment attenuation (α_s) as a function of sediment type, n_g, and bubble radius (r_o) using Equation 5, the steps outlined in Text S3, and the parameters listed in Tables S2 and S5 in Supporting Information S1 (Anderson & Hampton, 1980b):

$$\alpha_s = \frac{\pi f}{c_0}\left(\frac{c}{c_0}\right)\left[\frac{KY_1}{\gamma P_0 + \frac{4}{3}G}\right] \tag{5}$$

where α_s is attenuation in nepers per centimeter, c and c_0 are the fully saturated and gassy sediment sound speeds, respectively, K is the saturated sediment bulk modulus, and Y_1 is a calculated parameter which is highly dependent on the sediment n_g (see equations in SI Text S3).

Our results showed that α_s is more sensitive to n_g than r_o as the values of α_s begin to plateau at $r_o \sim 2$ mm for all n_g (Figure S10 in Supporting Information S1). Because there is generally a higher density of smaller bubbles in sediments and the acoustic backscatter return is a summation of the combined effects of various bubble sizes in the population (Anderson et al., 1998; Lyons et al., 1996), we took an average bubble radius of 1.5 mm for our ensuing calculations of α_s. We then corrected the measured Sv_{max} values for attenuation effects using Equation 6a and 6b to create Figure 4.

$$Sv_{max-new} = Sv_{max} + 2TL_b \tag{6a}$$

$$Sv_{max} = EL - SL + 2TL_w - T - E \tag{6b}$$

Here, EL and SL are the echo and source levels, respectively; $2TL_w$ is the two-way transmission loss consisting of geometrical spreading (ensures that identical reflecting targets produce the same echo strength regardless of their distance to the echo sounder) and acoustic attenuation of the sound energy in the water column; $T = 10log(c\tau/2)$, where c is speed of sound in the medium and τ is the transmitted pulse length; $E = 10log(\Psi)$, where Ψ is the solid angle of the equivalent beam pattern of the transducer, and $2TL_b$ is the two-way transmission loss due to gassy sediments as a function of the bubble radius and gas fraction (see Text S3 in Supporting Information S1).

Figure 1 shows the new GFR model relationships between $Sv_{max\text{-}new}$ and the observed sediment gas content. Due to the coarse resolution of our sediment sampling, the gas samples are split into four categories according to their sediment type (d50) and n_g. The final linear regressions for each of these categories are listed below:

$$\begin{aligned} &\text{For Silty Clay } n_g < 0.1 \\ &\qquad\qquad G = e^{(0.098 * Sv_{max} - 0.56)} \\ &\text{Silty Sand } n_g < 0.02 \end{aligned} \tag{7}$$

$$\text{For Silty Clay } n_g \geq 0.1 \quad G = e^{(0.008 * Sv_{max} + 1.40)} \tag{8}$$

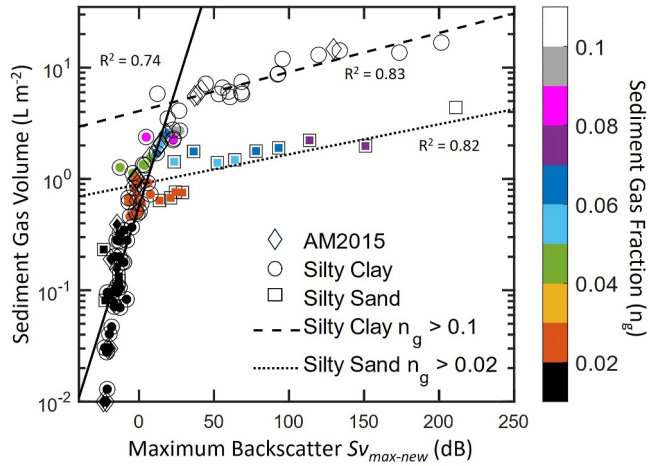

Figure 1. Sediment gas volume versus $Sv_{max\text{-}new}$ (old Sv_{max} corrected for sediment attenuation according to the sediment type and n_g). The solid black line (Equation 7) represents all low gas fraction data ($n_g < 0.1$ for silty clays and $n_g < 0.02$ for silty sands); the dashed black line (Equation 8) represents high gas fraction ($n_g > 0.1$) data for silty clays; and the dotted black line (Equation 9) represents high gas fraction ($n_g > 0.02$) data for silty sands.

$$\text{For Silty Sand } n_g \geq 0.02 \quad G = e^{(0.006 * Sv_{max} - 0.11)} \tag{9}$$

$$\text{For Sandy Gravel} \quad G \sim 0 \tag{10}$$

Due to the absence of discernible patterns in the sandy gravel sediments and the prevalent occurrence of 0-mL gas measurements across most of its sites ($n = 11$ out of 15), we inferred that the gas contribution from sandy gravel sediments is minimal (Equation 10).

4. Results

4.1. Sediment Characterization

4.1.1. Particle Size

In most sediment samples taken for this study, the silt fraction was predominant. It accounted for 74.5% of the average volume percent, with a minimum of 4.2% and a maximum of 91.9% (Table 2). While most of the samples comprised silty clay (deep and middle site samples), the shallow site samples contained a majority of coarser silty sand material. Figure 2 showcases the results of the Visual Aquatic (BioSonics, Seattle, WA, USA) Fuzzy C analysis for Uvas Reservoir (our main study reservoir). This clustering analysis, when compared to the sediment grab sample d50 data, revealed that the bottom sediments of each reservoir could be classified into 3 distinct sediment types: silty sands characterized by d50 particle sizes >63 μm; silty clays composed of d50 particle sizes <63 μm; and sandy gravel, primarily consisting of larger sand and gravel grain sizes. Due to the challenging nature of characterizing the sandy gravel sediment through grab samples using an Ekman-Birge grab sampler, visual inspection was employed when the reservoir water level was sufficiently low to expose the area (see Figure S5 in Supporting Information S1 for images). In this study, the silty clay samples had an average composition of 82% silt, 13% clay, and 3% sand, meaning that over 90% of the sediment consisted of particles less than 63 μm. Similarly, AM2015's study samples also consisted of sediments where over 90% of the particles had a diameter below 63 μm (the threshold separating silty clay and silty sand sediments).

4.1.2. Sediment LOI, OrgC, and Water Content

Due to field and laboratory constraints, LOI and water content (% H_2O) were only measured for the California reservoirs, while organic carbon content (OrgC) was assessed across all study reservoirs. % H_2O varied widely within each reservoir, with the lowest values (e.g., 18%) measured in shallow silty sand samples and the highest

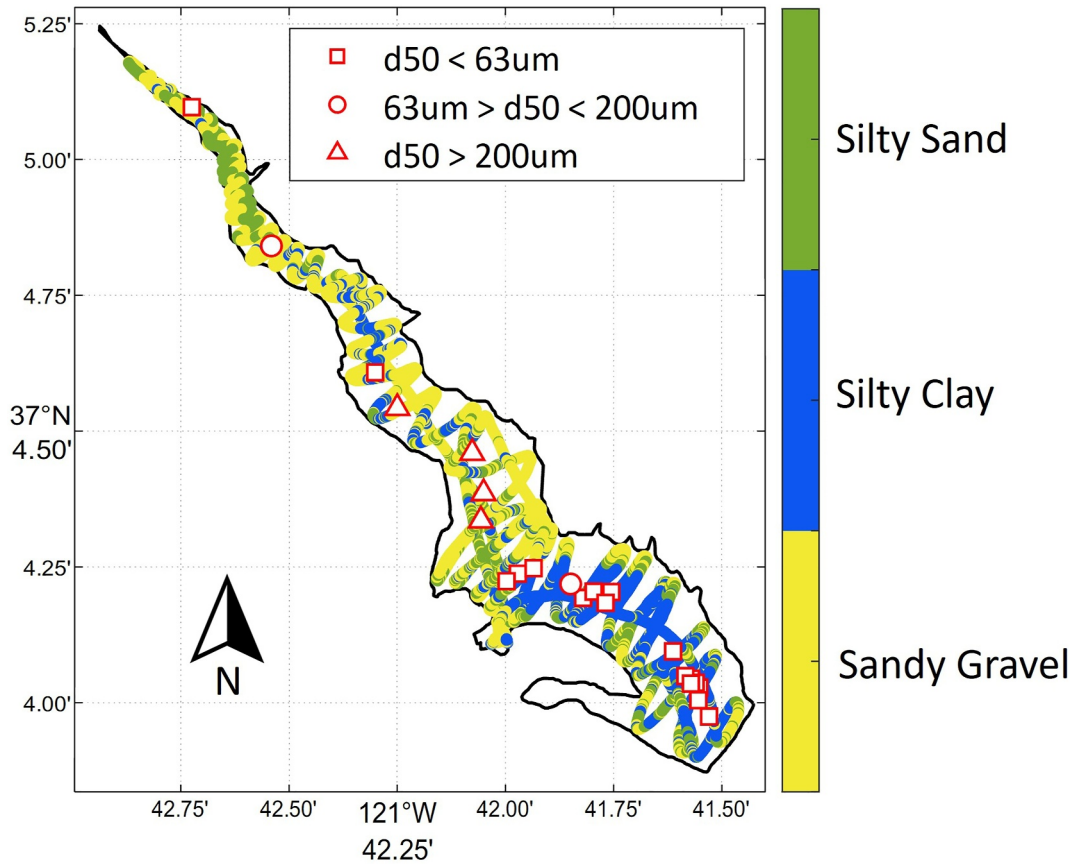

Figure 2. The BioSonics Visual Acquisition Fuzzy-C clustering output for Uvas Reservoir sediment type overlaid with in situ sediment d50 particle size data.

(e.g., 74.1%) in the deeper silty clay samples, yielding an average of 60.3% across all samples (Table 2). LOI ranged from a maximum value of 12.2% to a minimum value of 2.7% across the California reservoirs. The highest average LOI values were observed in Almaden, Chesbro, and Uvas (8.5%–10%), while Stevens had a lower average value of 7.2% (Table S7 in Supporting Information S1).

The sediment organic carbon content (OrgC) ranged from 0.3% in the shallow sediments of Almaden to 5.2% in the deep sediments of Uvas, with an overall average of 2.4% across all samples (Table 2, Table S7 in Supporting Information S1). OrgC values for Cubillas and Iznájar were consistent with this average. There was a significant positive correlation between OrgC and LOI (Spearman correlation $rs = 0.57$ and $p < 0.05$). Spatially, both the OrgC content and LOI in the sediments were higher in the silty clay classified samples (deeper regions closer to the dam) than in the upstream silty sand locations closer to the river inflows. However, neither % H_2O, LOI, or OrgC showed a significant correlation with sediment gas content.

4.1.3. Gas Content in the Sediment

The free gas content ranged from 0 to 16.75 L m^{-2} in the discrete sediment samples, with the lowest values found near the reservoir banks with sandy gravel sediments. The average CH_4 fraction within the gas bubbles sampled across all the reservoirs varied from 0% in Almaden Reservoir to 89.7% in Iznájar Reservoir with a mean value of 56.8 ± 29.2%. Gas volume negatively correlated with water depth ($rs = -0.42$ and $p < 0.05$), and varied according to the seasons, showing a strong positive correlation with BWT ($rs = 0.63$ and $p < 0.05$) (see Table 3). The gas-to-sediment ratio n_g within the sediments ranged from values as low as 0.001 to a maximum value of 0.559 found in Cubillas Reservoir (see Figure S6 in Supporting Information S1). On average, most samples classified as silty clay had n_g values < 0.1, with exceptions occurring in samples that (a) had a water depth range

Table 3

The Spearman Rank Correlation Coefficients (rs) Between the Measured Sediment Characteristics, Sediment Gas Volume, Bottom Water Temperature (BWT), Dissolved Oxygen Near the Sediments (DO_{bottom}) Against the Measured Values for Maximum Backscatter Strength (Sv_{max}), Second Part of the First Bottom Echo (E1), First Part of the First Bottom Echo (E1′), and Acoustic Fractal Dimension (FD)

	Gas (L m^{-2})	Water depth (m)	H_2O (%)	LOI (%)	OrgC (%)	Clay (%)	Silt (%)	Sand (%)	BWT (°C)	DO_{bottom} (mg L^{-1})
Sv_{max}	**0.38**	0.21	0.27	–	−0.29	0.40	–	−0.37	–	–
E1	–	0.47	0.47	–	**−0.48**	0.69	–	−0.62	–	–
E1'	–	0.47	0.37	–	−0.44	0.52	–	−0.43	–	–
FD	–	**0.66**	**0.65**	–	−0.40	**0.71**	**0.46**	**−0.80**	−0.36	–
Gas (L m^{-2})	–	−0.42	–	–	–	–	–	–	**0.63**	−0.26

Note. In each case, the *rs* had a significance value < 0.05, and bolded values highlight the highest *rs* value for each sediment characteristic ($n = 169$).

between 1.9 and 5.4 m (which is shallower than most of the silty clay samples) and (b) came from highly productive eutrophic systems at a time when the BWTs were above 20°C. These outlier samples (most of them occurring in Cubillas Reservoir) also exhibited lower than expected Sv_{max} values (diamonds in Figure 3a). On the other hand, all the samples measured by AM2015 (and classified as silty clay) had n_g values < 0.1 with only four being greater (circled stars in Figure 3a and white diamonds in Figure S6 in Supporting Information S1). The depths of these data points range between 8 and 20 m, which is much higher than 5.4 m (the maximum depth of our samples with $n_g > 0.1$). Only one of the high gas samples matches the AM2015 study's depth range and falls within their four high gas data points (see the circled blue triangle in Figure 3a). This sample corresponds to a silty clay sample from Uvas Reservoir, with a water depth above the sediment of ≈10 m.

Silty sand samples had n_g values that ranged from 0.001 to 0.280 with an average n_g of 0.04, with higher volume samples also exhibiting lower than expected Sv_{max}. Like the silty clay samples, these outlier silty sand samples had total water depths below 5 m or BWTs above 20°C or both. Similar to gas volume, n_g showed a strong positive correlation to temperature ($rs = 0.59$ and $p < 0.05$, see Figure S7 in Supporting Information S1) as well as a negative correlation to bottom water DO ($rs = -0.36$ and $p < 0.05$).

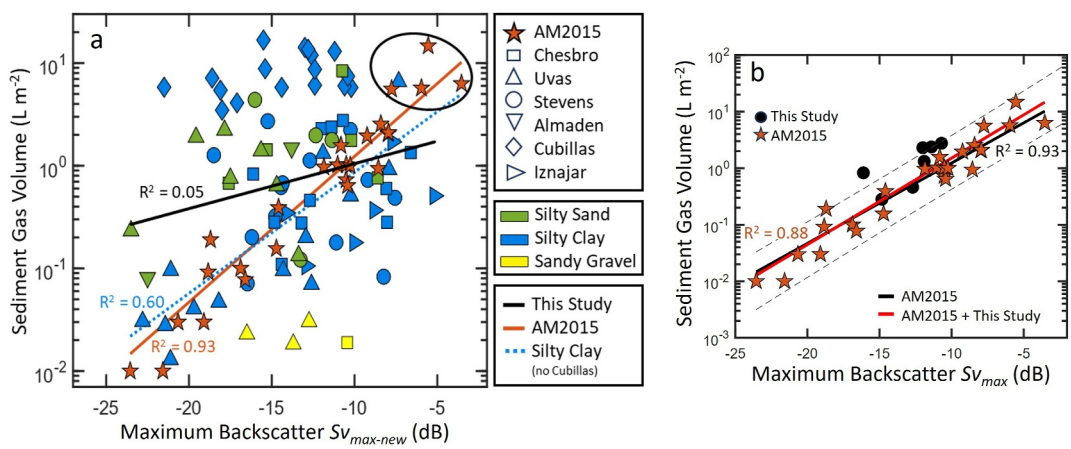

Figure 3. (a) Gas volume in surficial sediments versus Sv_{max}. The red line represents the AM2015 relationship ($y = \exp^{0.327Sv_{max}+3.48}$), the solid black line ($y = \exp^{0.105Sv_{max}+1.05}$) represents the relationship according to **all** the data collected in this study, and the dotted blue line ($y = \exp^{0.271Sv_{max}+2.57}$) depicts the linear fit of **only** the silty clay sediments (excluding the Cubillas data). The encircled data represent the AM2015 data that have a gas fraction (n_g) higher than 0.1. (b) Gas volume in surficial sediments versus Sv_{max} at 201 kHz for cohesive sediments. The black circles represent data from this study that had greater than 60% water content and 2% OrgC (as per the AM2015 requirements). The black line ($y = \exp^{0.327Sv_{max}+3.48}$) represents the original AM2015 regression with 95% confidence intervals plotted in gray, and the red line ($y = \exp^{0.352Sv_{max}+3.93}$) represents the new regression when red and black data points are combined.

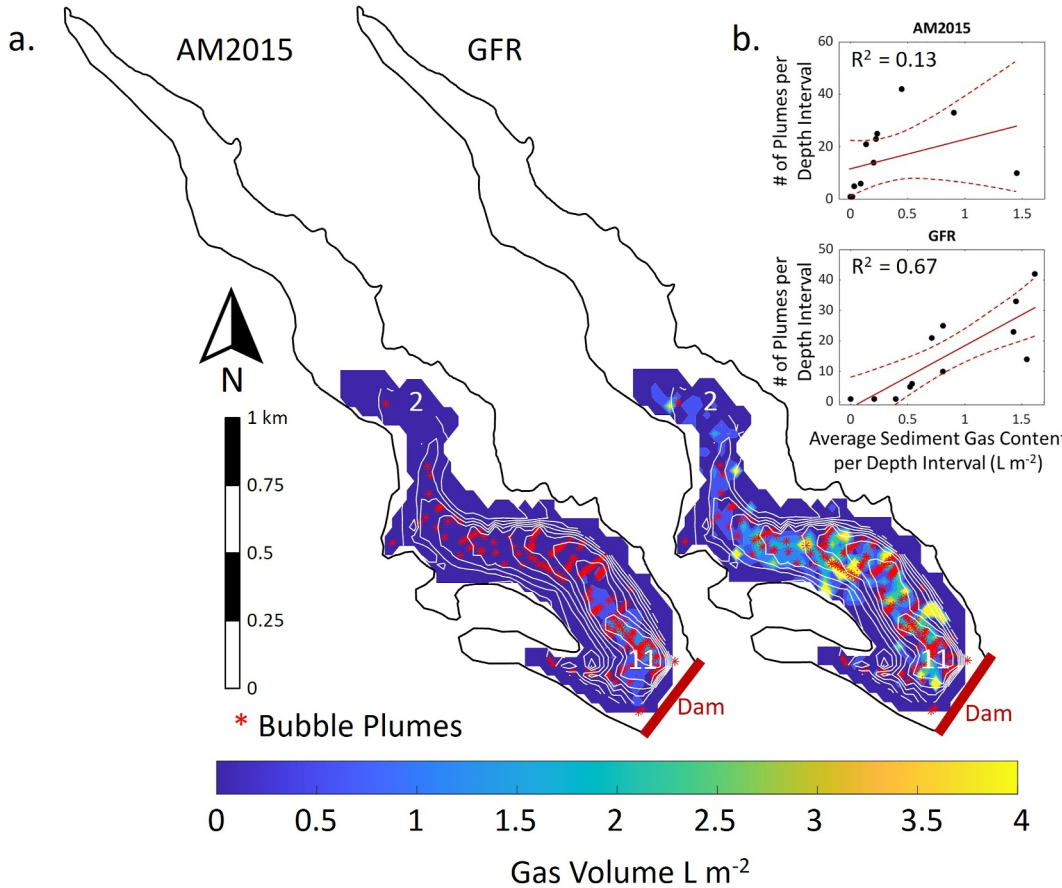

Figure 4. (a) Sediment gas volume distribution for Uvas Reservoir during the 30 July 2021 survey according to the AM2015 (left) and GFR (right) models. Water depth contours are in white and occur every 1 m. (b) Total number of bubble plumes versus average sediment gas content per each water depth bin (white contour lines) for the AM2015 (top) and GFR (bottom) models. Dotted red lines represent the 95% confidence intervals for the correlation lines (solid red).

4.2. Acoustic Models for the Prediction of Gas Content in the Sediment

4.2.1. Influence of Acoustic Configuration Settings on Sv_{max}

The experiment carried out in fall 2023 in Cubillas Reservoir revealed that changes to certain configuration settings had significant effects on the Sv_{max} output. Specifically, it showed that changing the pulse duration (τ) of the sonar from 0.5 to 0.1 ms provided an average of +6 dB to all samples along the transect. A change from 0.5 to 0.3 ms had an average of +2 dB. In contrast, changing the ping rate from five pings s^{-1} to three pings s^{-1} provided no discernible difference to the Sv_{max} output (see Text S1, Figure S8 in Supporting Information S1). As expected, changing the transmit power from 0 dB to −10 dB resulted in a −10 dB difference. These findings underscore the sensitivity of the Sv_{max} output to variations in sonar configuration settings, particularly pulse duration and transmit power, highlighting the importance of sonar settings in acoustic surveys of gassy sediments.

4.2.2. Acoustic Relationship to Sediment Properties

Of the acoustical properties (Table 3 and see example echogram in Figure S2 in Supporting Information S1), the fractal dimension (FD) was significantly correlated with several sediment properties including water depth ($rs = 0.66$), water content (% H_2O) ($rs = 0.65$), % OrgC ($rs = -0.40$), % Clay ($rs = 0.71$), % Silt ($rs = 0.46$), and % Sand ($rs = -0.80$). However, E1 was more strongly correlated with % OrgC ($rs = -0.48$) than FD. Sv_{max} is the only acoustic parameter with a significant correlation to gas volume ($rs = 0.38$, $p < 0.05$). In addition to having a strong correlation to gas content, Sv_{max} is also correlated to water depth ($rs = 0.21$), % H_2O ($rs = 0.27$), and % Clay ($rs = 0.40$) as well as strongly dependent on E1 and E1′ ($rs = 0.84$ and 0.88, respectively; see Figure S8 in

Table 4
The Calculated Mean Absolute Error (MAE), Root Mean Squared Error (RMSE), and % Error From the AM2015 and GFR Model Outputs

Model	Sediment type	MAE	RMSE	% error
AM2015	All	2.11	3.88	224
	Sandy Gravel	1.04	1.33	9,454
	Silty Clay	2.96	4.88	194
	Silty Sand	1.43	2.24	99
GFR	All	0.49	0.91	57
	Sandy Gravel	0.01	0.01	26
	Silty Clay	0.68	1.16	56
	Silty Sand	0.35	0.46	28

Supporting Information S1). From these observations and the correlations reported in Section 4.1.3, it became evident that characteristics such as sediment type, gas fraction (n_g), and water depth play a role in the acoustic return of gassy sediments, whereas BWT and DO most likely relate to the rate of production, solubility, and consumption of the gas at depth.

4.2.3. AM2015 and GFR Model Evaluation

In their 2015 work, AM2015 only included samples that contained >60% water content and >2% OrgC content to predict gas storage in the sediment as a function of Sv_{max}. Only seven samples in our data set satisfied these criteria. They are plotted in Figure 3b together with the AM2015 data. The linear fit of those seven samples together with those from AM2015 is similar to that proposed earlier by AM2015 (slope of 0.352 vs. 0.327 and y-intercept of 3.93 vs. 3.48) with a minimally reduced explained variance of 88% versus 93% ($R^2 = 0.88$ vs. 0.93). However, when our full data set was included (independently of water or organic carbon content), the regression's R^2 value decreased to 0.18, explaining only ∼18% of the variance in samples and 5% of the variance when excluding the AM2015 data ($R^2 = 0.05$) (Figure 3a). Hence, water and carbon content in sediments can strongly limit the applicable range of the AM2015 relation. Finally, data points from this study's California reservoirs and Iznájar Reservoir (all the silty clay data except the outlying blue diamonds representing Cubillas Reservoir) showed good alignment ($R^2 = 0.60$) with the data collected by AM2015 (Figure 3a).

Unlike AM2015, the GFR model offers new regressions (Equations 7–10) that offer better explanations for the data variability presented in Figure 3a. By correcting for gas and sediment type attenuation effects (Figure 1), the GFR model yields significantly improved R^2 values: Equation 7—$R^2 = 0.74$, Equation 8—$R^2 = 0.83$, and Equation 9—$R^2 = 0.82$. Furthermore, the GFR model effectively categorizes data based on sediment and gas content, revealing distinct behavior in saturation thresholds across different sediment types. It also surpasses the AM2015 model in terms of predictive accuracy, with an RMSE of 0.91, MAE of 0.49%, and 57% error, compared to AM2015's RMSE of 3.88, MAE of 2.11%, and 224% error (Table 4).

4.3. Sediment Gas Distribution and Bubble Plumes: AM2015 Versus GFR Models

The mass of CH_4 in the bottom sediments of Uvas Reservoir during the summer 2021 survey was calculated by multiplying the gas volume in each grid cell by the grid size and then converting the results to mass using the average CH_4 fraction in the sediments (40.2 ± 32.8%). This value is consistent with Marcon et al. (2023), who reported a CH_4 fraction of 58%. According to the AM2015 model, the total CH_4 content in the sediments is approximately 44.6 kg. In contrast, the GFR model estimates a much higher total of 126.8 kg (see Figure S11 in Supporting Information S1), highlighting a substantial discrepancy between the two models.

Both the AM2015 and GFR models were used to generate sediment gas content maps for the Uvas Reservoir survey on 30 July 2021 (Figure 4a). The reservoir, at the time, had a maximum depth of around 12 m and an average depth of ≈5 m, with the deepest area located in the southern-southeastern portion. For individual grid cell predictions, the AM2015 model estimated gas volumes ranging from 0 to 2.5 L m^{-2}, with an average of 0.31 L m^{-2}. In comparison, the GFR model predicted a wider range of 0–10.98 L m^{-2}, with volumes between 0.5

and 3 L m^{-2} being more common across most of the lake. These values are similar to those reported by Anderson and Martinez (2015) for Lake Elsinore, where gas volumes ranged from 0 to 10 L m^{-2}, with averages between 2 and 3 L m^{-2}.

Significant spatial variability in sediment gas content was observed. The AM2015 model showed a strong correlation between gas volume and depth, with the highest values (1–2.5 L m^{-2}) near the dam at water depths of 10–12 m. In contrast, the GFR model predicted gas volumes on the order of 2.5 L m^{-2} as shallow as 5 m, with the highest gas volumes (>4 L m^{-2}) mainly occurring between the 7 and 9 m depth contours (Figure 4a). The bubble plume count per bin was lowest in shallow areas, peaking at 10 m before decreasing again at 11 and 12 m (Figure S12 in Supporting Information S1). Despite the highest gas content predictions (7–9 m) not aligning with the location of the highest bubble plume count (10–11 m), the GFR model's gas content prediction aligned well with observed bubble plumes, achieving an R^2 of 0.67 (p-value <0.01) (see Figure 4a, red stars, and data in Figure 4b). Meanwhile, the AM2015 model showed no significant correlation between gas content and bubble plume location ($R^2 = 0.13$ and p-value = 0.25), struggling to predict the location of bubbling hotspots, particularly upstream of the dam at depths of less than 10 m, where ebullition was observed, but gas predictions were negligible (<0.2 L m^{-2}) (Figures 4a and 4b). This highlights the AM2015 model's limitations in accounting for the spatial variability across different sediment types.

5. Discussion

5.1. Limitation of the Existing AM2015 Model and Improvement With the GFR Model

In 2015, AM2015 proposed a model for estimating total gas volume in surficial organic sediments, primarily applicable to deeper fine-grained sediments. However, our study reveals limitations in its applicability to shallow, sandy, or highly gassy sediments, prompting the development of the GFR model. The GFR model offers improvements by incorporating the sound attenuation in the sediment as a function of sediment type, average bubble radius, and sediment gas fraction (n_g) as a correction factor for gas effects on the backscatter strength of shallow sediments. Figure 1 reveals an important finding regarding the acoustic relationship between Sv_{max} and gas content. Note first that the data in Figure 1 display positive Sv_{max} values. This has been observed previously in the presence of highly reflective substrates such as bubbles in water due to substantial turbulence, such as hydrothermal gas vents (Deimling et al., 2010) and wind induced surface bubbles (Dalen & Løvik, 1981), or other instances of highly gaseous sediments (Tegowski et al., 2006). More importantly though, the data (Figure 1) reveal a distinct variation in the behavior of two sediment types: silty sand and silty clay. Notably, the silty sand samples deviate significantly from the primary Sv_{max}—gas content relationship (Equation 7) at a much lower gas fraction threshold ($n_g = 0.02$) than the silty clay samples, which exhibit this departure at a higher gas fraction threshold ($n_g = 0.1$). This discrepancy can be attributed to the inherent disparities in the physical characteristics of these two sediment types. The silty sand, being coarser and more porous, has a lower gas-holding capacity than the denser silty clay. As a result, gas bubbles escape more easily from the sand matrix than from the clay, leading to a lower gas saturation point ($n_g = 0.02$). Furthermore, it is evident that once each sediment type approaches its respective saturation limit, the slope of the regression line (Equations 8 and 9) experiences a significant decrease toward zero and the change in gas content remains within one order of magnitude. This behavior is likely due to the equilibrium that develops between the rate of gas production and the rate of gas release (i.e., bubbling) as the respective sediment gas fractions approach their saturation thresholds.

Spatial variations in estimated sediment gas content are correlated with sediment type, water depth, BWT, and DO. The gas content was negatively correlated to water depth and DO ($rs = -0.42$, $p < 0.05$ and $rs = -0.26$, and $p < 0.05$), and positively correlated to BWT ($rs = 0.63$ $p < 0.05$) and % silt in the sediments ($rs = 0.26$, $p < 0.1$). We speculate that the negative correlation between water depth and gas content could account for hydrostatic pressure, as well as an indirect measure of sediment temperature (colder at the deepest depths). Considering these relationships, the GFR model outperforms the AM2015 model in predicting gas content (Table 4) since it accounts for the spatial variation according to the sediment type.

Interestingly, we observed that the highest frequency of significant errors in predicting sediment gas content occurred at locations where the reservoir sediment type transitions from one type to another. This was particularly pronounced for silty clay classified sediments situated near regions of steeper slopes, with percent errors reaching 57%, as opposed to 26% and 28% for sandy gravel and silty sand, respectively. It is a known fact that steep slopes can significantly affect acoustic backscatter measurements of bottom sediments (Sternlicht & de Moustier, 2003).

This observation underscores the rationale behind our application of a slope threshold in our spatial analysis. Furthermore, though the GFR model accounted for the sediment type heterogeneity by using fuzzy logic to compute the total sediment attenuation, it is plausible that at these transition zones, the sediment type exhibits greater heterogeneity than the GFR model can accurately estimate. An avenue for enhancing the GFR model's accuracy could involve running sonar transects at a higher spatial resolution to account for the small-scale sediment type heterogeneity.

5.2. Gas Content and Sediment Instability: Evaluations From Uvas Reservoir and Related Studies

To further explore the implications of our findings, we can examine the gas fractions predicted by the GFR model in the context of sediment characteristics and comparable studies. Assuming the gas content is concentrated within the top 10 cm of sediment, the GFR predicted volumetric gas fractions for Uvas Reservoir range from 0% to 10.98%, with an average of 1.39. These fractions are similar to those reported for Lake Kinneret (0.2%–3.8% Katsnelson et al., 2017; Uzhansky et al., 2020). They also fall within the range observed for Lake Passaúna, where gas fractions varied from 0.1% – 40.1%, with sediments of lower wet bulk density showing relatively less gas content (Marcon et al., 2022). However, comparing the Marcon et al. (2022) data to ours is questionable due to differences in methodology. In Section 4.2.1, we demonstrated that Sv_{max} is sensitive to the pulse duration setting. Marcon et al. (2022) used a pulse duration of 0.13 ms versus the 0.4-ms setting used in this study and by Anderson and Martinez (2015).

When considering the broader implications for sediment stability and gas ebullition, previous studies by van Kessel and van Kesteren (2002) and Liu et al. (2018) suggest that gas voids can destabilize sediments by reducing wet bulk density, ultimately leading to gas release by bubbling. van Kessel and van Kesteren (2002) specifically found that gas content between 25% and 37% could trigger instability in muddy sediments. Interestingly, in Uvas Reservoir, none of the grid cells had a gas content greater than 11%, with most cells ranging between 0.5% and 3%. Despite this, we observed active ebullition in areas with gas content below the 25% threshold suggested by van Kessel and van Kesteren (2002), as highlighted by red stars in Figure 4a and data in Figure 4b. This challenges the notion of a fixed gas saturation threshold for ebullition, suggesting that other factors, such as sediment composition or gas distribution, may play a more significant role in triggering bubble release.

Liu et al. (2016) provide additional insight by demonstrating that ebullition can occur even at low gas content, though substantial bubbling tends to arise when the ratio of ebullition to sediment CH_4 production exceeds 20%. Their findings suggest that significant ebullition occurs when gas fractions reach approximately 12% for clay, 8% for silt, and 5% for sand. In the case of Uvas Reservoir, the few cells with the highest gas content (~1%) fall within the range Liu et al. (2016) reported for silt sediments, suggesting that even small pockets of gas can trigger bubbling, especially in fine-grained sediments.

Overall, these findings suggest that while the GFR model's predictions of gas content are consistent with other studies, the dynamics of ebullition and sediment instability may be more complex than previously thought. Gas content alone may not fully explain the spatial patterns of ebullition, and other factors, such as sediment texture, local hydrodynamics, and reservoir operations (i.e., water level drawdowns), may influence the release of gas from sediments.

5.3. Spatial Distribution of Sediment Gas Content Compared to Bubble Plume Location

The GFR distribution of gas within the sediments of Uvas Reservoir from the July 2021 survey exhibits high spatial heterogeneity affecting the spatial variability of ebullition. Longitudinally, the largest amount of gas in the sediment was detected in the downstream part of the reservoir, located between the 7 and 9 m depth contours (Figure 4a), in a region where the discrete sediment samples indicated a higher silt content. Conversely, sediments next to the dam that exhibit more clay-like textures (d90 < 20 μm), and the larger sediments (d90 > 200 μm) closer to the inlet and littoral zones (Figure S12 in Supporting Information S1) show less gas volume. Previous research has suggested that sediments containing elevated levels of silt impede CH_4 ebullition (Martinez & Anderson, 2013). This, coupled with increased bottom temperatures and an oxycline depth of 5.5 m (the water depth at which DO falls below 2 mg L^{-1}, as per Nürnberg, 2004, see Figure S13 in Supporting Information S1), provides a plausible explanation for the heightened gas content found predominantly in the region between the 7 and 9 m depth contours. This observation is further supported by the fact that the deeper clay sediments also contain higher gas content than the shallower silty sand sediments. Though gas content was positively correlated with

temperature, none of the discrete gas samples existing above the oxycline depth had n_g values > 0.1, supporting the fact that CH_4 production is less likely to occur in oxic conditions even though temperatures are high enough to support microbial activity. Conversely, even when DO levels indicate anoxic conditions, CH_4 production is limited by BWTs (see Figure 4a, depth contours greater than 9 m).

The absence of gas ebullition in the littoral sediments is contrary to what has been observed in other lakes and reservoirs, where ebullition is often found most active in the littoral zones (Martinez & Anderson, 2013; Natchimuthu et al., 2016; Wik et al., 2013), but does align with findings in Lake Kinneret (Liu et al., 2020). This is likely influenced by the fact that the sediments in shallower regions experience warmer temperatures earlier in the year compared to deep sediments. This early warming facilitates the onset of CH_4 production sooner in shallower sediments as temperature is likely the main driver of methane production (DelSontro et al., 2016; Duc et al., 2010; Liu et al., 2016). Additionally, these shallower sediments encounter lower hydrostatic pressures, requiring a lower concentration of dissolved gas to reach oversaturation and therefore bubble formation (Liu et al., 2016). This is further confirmed in Figure 1, where the silty sand sediments demonstrate a clear breaking point that is lower than the breaking point for the silty clay sediments ($n_g = 0.02$ instead of 0.1). Figure 2 also suggests this as the littoral zones in Uvas Reservoir predominantly consist of larger particle-sized sediments (like Lake Kinneret per Liu et al., 2020). Consequently, this allows the sediment gas from shallow zones to escape earlier in the year (i.e., spring instead of summer) than the gas in deeper zones. The predicted gas content modeled in Figure 4 is from a summer survey conducted at Uvas Reservoir. As such, it is likely that by the time of the survey, the shallow sediments had already depleted their sediment OrgC stores, meaning that the cycle of GHG production and ebullition most likely occurred in the spring instead of the summer and fall. Finally, although this study did not resolve the small-scale variability of gas content in sediment, primarily due to limitations like the sonar footprint (which varies with water depth) and data averaging within grid cells, it does underscore the importance of conducting hydroacoustic surveys for detecting spatial patterns in gas content. Such patterns may go unnoticed when relying solely on sampling at discrete locations.

5.4. Further Considerations and Limitations

In this study, we derived gas content in the sediment from acoustic measurements, focusing on Mediterranean climate reservoirs. While our study provided valuable insights into the spatial distribution of sediment gas content and its qualitative relationship to ebullition, it also has some limitations and considerations for future research. For example, in this investigation, because we only had discrete measurements of n_g, we used BWT ($rs = 0.56$, $p < 0.01$; Figure S14 in Supporting Information S1, see Text S4 in Supporting Information S1 for more detail) as a first approximation to model its spatial variability for the summer 2021 survey at Uvas Reservoir. These estimated n_g values were then used to predict the sediment gas content (Figure 4) according to the GFR model presented in Figure 1. Although other variables were tested against the measured n_g, only BWT showed a significant correlation with an R^2 value higher than 0.5. The total prediction error for sediment gas content was 57% when n_g is known (Table 4), but increases by 20% when using the BWT–n_g relationship described in the Supplementary Information (see Text S4 in Supporting Information S1). The inherent uncertainty in this initial prediction of n_g may lead to a reduced accuracy in the total sediment gas content when applying the GFR model on a large spatial scale. However, even with the BWT-based n_g estimates, the GFR model outperforms the AM2015 model by incorporating sediment type, which is crucial for predicting and understanding sediment gas content. Future research should prioritize developing more robust relations for gas content predictions according to sediment type and other influential factors (e.g., reservoir trophic status).

Moreover, measurements were made at sites with depths greater than 1.6 m, due to the anticipated limitations of sound wave propagation at depths shallower than this threshold. While minimal gas content was indicated in sediments below this depth (<1.6 m) in our California reservoirs, it is crucial to recognize that shallow fine-grained systems, such as Cubillas, might harbor substantial gas storage that the depth limitations of the acoustic method may inaccurately quantify. Additionally, data were excluded from areas with slope angles exceeding 10° (Anderson et al., 2007; Boyle & Chotiros, 1995; Fonseca et al., 2002; Huang et al., 2018; Marcon et al., 2022; Sternlicht & de Moustier, 2003). In mountainous terrains like that of Uvas Reservoir, the bathymetric topography often includes sloped sides exceeding our chosen threshold. While it is unlikely that such regions are prone to substantial CH_4 gas production, the percent error in the GFR silty clay sediment results suggest high uncertainty in these areas, which future studies should aim to better characterize. Furthermore, our use of a relatively high frequency (201 kHz) specifically quantifies gas in surficial sediments (Anderson & Martinez, 2015) and may not

be suitable for sediments with a deeper gassy layer. The depth of Sv_{max} measured by our sonar and observed in the echograms ranged from 2 to 50 cm below the sediment-water interface (Figures S2 and S3 in Supporting Information S1), with an average depth of ∼25 cm, consistent with sediment depths observed by Liu et al. (2016) and modeled by Langenegger et al. (2019). However, some studies suggest that methane gas can reside up to 1 m below the sediment-water interface (Liu et al., 2020). Lower frequencies could potentially resolve such features, as demonstrated by Schneider von Deimling et al. (2013). Nevertheless, for most freshwater systems, measuring gas within surficial sediments is appropriate, as methanogenesis typically occurs near the sediment-water interface (Langenegger et al., 2019; Marcon et al., 2023) which is the region most closely associated with ebullition (Anderson & Martinez, 2015; Martinez & Anderson, 2013).

Finally, to enhance our understanding of the spatial variability and temporal dynamics of CH_4 fluxes in inland waters, it is imperative to continue investigating the processes governing CH_4 production, storage, transport, oxidation, and emission. High-resolution acoustic surveys hold promise in providing estimates of sediment gas content and its spatial and temporal variations. Furthermore, extending the application of echo sounding and ebullition monitoring to encompass more sampling locations is essential for delving into the nuanced connections between gas storage and ebullition, as exemplified in this investigation (e.g., Cubillas). Nonetheless, it is imperative that such monitoring employs consistent acoustic frequencies and configuration settings (see Section 4.2.1). Without this uniformity, cross-comparing studies becomes challenging, rendering models ineffective for predicting gas content.

6. Conclusions

Our exploration of the AM2015 model has exposed its limitations, particularly when applied to shallow, sandy, or highly gassy fine-grained sediments. These findings bear substantial implications for our ability to accurately estimate gas content in sediments, especially in shallow waters. In addressing these challenges, we presented an explanation for the observed deviation in acoustic behavior within these highly gaseous, shallow environments, attributing it to attenuation within the sediments because of the gas itself. As a result, we extended the AM2015 model to an improved model (GFR) that incorporates n_g and sediment type as a correction factor for gas attenuation effects on the Sv_{max} values. The results of the extended model improved the gas volume data dispersion found in Figure 3a to reveal four distinct and clearer trends in Figure 1. This approach also facilitates a more comprehensive understanding of how gas is stored in various sediment types, offering valuable insights for further analysis and decision-making processes. The absence of gas and ebullition in littoral sediments, contrary to typical observations in other aquatic environments, emphasizes the necessity for a nuanced understanding of sediment properties, basin topography, and water conditions. Additionally, the challenges in accurately characterizing sediment type transitions and small-scale variability underscore the importance of hydroacoustic surveys for detecting spatial patterns that might be missed through discrete sampling. Looking ahead, it is imperative to continue investigating the processes governing GHG production, storage, transport, and emission in inland waters, with a focus on refining models and expanding the scope of acoustic measurements. This research avenue holds the potential to enhance our understanding of the dynamic nature of gas content in sediments and its role in CH_4 fluxes, ultimately contributing to more accurate assessments of greenhouse gas emissions from aquatic ecosystems.

Conflict of Interest

The authors declare no conflicts of interest relevant to this study.

Data Availability Statement

Data were deposited in the Hydroshare data repository operated by The Consortium of Universities for the Advancement of Hydrologic Science Inc. (CUAHSI) with the following citation:

Thirkill, R. H., Ramon, C. L., Oldroyd, H. J., Seelos, M., Rueda, F. J., & Forrest, A. L. (2024). Quantifying Methane in Mediterranean-climate Reservoirs. HydroShare. https://doi.org/10.4211/hs.f515894114b04850b8af564bf425f672.

Acknowledgments

This study was funded by the Valley Water Agency, in Santa Clara County, the American Geophysical Union through the Horton Research Grant (2021), projects COSTUMER (ref. P21_00238) and QUAL21-011 (Modeling Nature) through the Regional Government of Andalusia (Junta de Andalucía, Consejería de Universidad, and Investigación e Innovación), projects CRONOS (RTI2018-098849-B-I00), and ANTICIPA (PID2022- 137865OB-I00) through the Spanish Ministry of Science, Innovation and Universities, and the University of California, Davis Office of Global Affairs Seed Grant Program for International Activities. The authors thank Corrin Clemons, Wilton Gray, Julianna Porraz and Kendall Galvez, Isabel Reche, Rafael Morales, and Andrés Martínez for their help and support with field campaigns, and Sergio Jimenez and Noah Skelly for assistance in the lab. The authors further thank Billy Tu, William DeDen, and Nina Trusso for their field support in the acoustic mapping of the Valley Water reservoirs and James Downing for offering them as a research base. Finally, we thank the anonymous reviewers and our editor for their helpful feedback, which helped us improve the manuscript.

References

Abegg, F., & Anderson, A. L. (1997). The acoustic turbid layer in muddy sediments of Eckernfoerde Bay, Western Baltic: Methane concentration, saturation and bubble characteristics. *Marine Geology, Gas in Marine Sediments, Geology/Geochemistry/Microbiology*, *137*(1–2), 137–147. https://doi.org/10.1016/S0025-3227(96)00084-9

Anderson, A. L., Abegg, F., Hawkins, J. A., Duncan, M. E., & Lyons, A. P. (1998). Bubble populations and acoustic interaction with the gassy floor of Eckernförde Bay. *Continental Shelf Research*, *18*(14–15), 1807–1838. https://doi.org/10.1016/S0278-4343(98)00059-4

Anderson, A. L., & Hampton, L. D. (1980a). Acoustics of gas-bearing sediments I. Background. *Journal of the Acoustical Society of America*, *67*(6), 1865–1889. https://doi.org/10.1121/1.384453

Anderson, A. L., & Hampton, L. D. (1980b). Acoustics of gas-bearing sediments. II. Measurements and models. *Journal of the Acoustical Society of America*, *67*(6), 1890–1903. https://doi.org/10.1121/1.384454

Anderson, J. T., Holliday, D. V., Kloser, R., Reid, D., Simard, Y., Brown, C., et al. (2007). Acoustic seabed classification of marine physical and biological landscapes.

Anderson, M. A., & Martinez, D. (2015). Methane gas in lake bottom sediments quantified using acoustic backscatter strength. *Journal of Soils and Sediments*, *15*(5), 1246–1255. https://doi.org/10.1007/s11368-015-1099-1

Barros, N., Cole, J. J., Tranvik, L. J., Prairie, Y. T., Bastviken, D., Huszar, V. L. M., et al. (2011). Carbon emission from hydroelectric reservoirs linked to reservoir age and latitude. *Nature Geoscience*, *4*(9), 593–596. https://doi.org/10.1038/ngeo1211

Bastviken, D., Cole, J., Pace, M., & Tranvik, L. (2004). Methane emissions from lakes: Dependence of lake characteristics, two regional assessments, and a global estimate. *Global Biogeochemical Cycles*, *18*(4). https://doi.org/10.1029/2004GB002238

Bastviken, D., Santoro, A. L., Marotta, H., Pinho, L. Q., Calheiros, D. F., Crill, P., & Enrich-Prast, A. (2010). Methane emissions from Pantanal, South America, during the low water season: Toward more comprehensive sampling. *Environmental Science and Technology*, *44*(14), 5450–5455. https://doi.org/10.1021/es1005048

Baudo, R. (2020). Sediment sampling, mapping, and data analysis. In R. Baudo, J. P. Giesy, & H. Muntau (Eds.), *Sediments* (pp. 15–60). CRC Press. https://doi.org/10.1201/9780367810894-2

Beaulieu, J. J., McManus, M. G., & Nietch, C. T. (2016). Estimates of reservoir methane emissions based on a spatially balanced probabilistic-survey. *Limnology & Oceanography*, *61*(S1), S27–S40. https://doi.org/10.1002/lno.10284

Biosonics, Inc. (2020). *User guide: Visual aquatic 1.10* (p. 56). BioSonics, Inc.

Blott, S. J., & Pye, K. (2012). Particle size scales and classification of sediment types based on particle size distributions: Review and recommended procedures. *Sedimentology*, *59*(7), 2071–2096. https://doi.org/10.1111/j.1365-3091.2012.01335.x

Boyle, F. A., & Chotiros, N. P. (1995). A model for high-frequency acoustic backscatter from gas bubbles in sandy sediments at shallow grazing angles. *Journal of the Acoustical Society of America*, *98*(1), 531–541. https://doi.org/10.1121/1.413645

Dalen, J., & Løvik, A. (1981). The influence of wind-induced bubbles on echo integration surveys. *Journal of the Acoustical Society of America*, *69*, 1653–1659. https://doi.org/10.1121/1.385943

Deemer, B. R., Harrison, J. A., Li, S., Beaulieu, J. J., DelSontro, T., Barros, N., et al. (2016). Greenhouse gas emissions from reservoir water surfaces: A new global synthesis. *BioScience*, *66*(11), 949–964. https://doi.org/10.1093/biosci/biw117

von Deimling, J. S., Greinert, J., Chapman, N. R., Rabbel, W., & Linke, P. (2010). Acoustic imaging of natural gas seepage in the North Sea: Sensing bubbles controlled by variable currents. *Limnology and Oceanography: Methods*, *8*(5), 155–171. https://doi.org/10.4319/lom.2010.8.155

DelSontro, T., Beaulieu, J. J., & Downing, J. A. (2018). Greenhouse gas emissions from lakes and impoundments: Upscaling in the face of global change. *Limnology and Oceanography Letters*, *3*, 64–75. https://doi.org/10.1002/lol2.10073

DelSontro, T., Boutet, L., St-Pierre, A., del Giorgio, P. A., & Prairie, Y. T. (2016). Methane ebullition and diffusion from northern ponds and lakes regulated by the interaction between temperature and system productivity. *Limnology & Oceanography*, *61*(S1), S62–S77. https://doi.org/10.1002/lno.10335

DelSontro, T., Kunz, M. J., Kempter, T., Wüest, A., Wehrli, B., & Senn, D. B. (2011). Spatial heterogeneity of methane ebullition in a large tropical reservoir. *Environmental Science and Technology*, *45*(23), 9866–9873. https://doi.org/10.1021/es2005545

DelSontro, T., McGinnis, D. F., Wehrli, B., & Ostrovsky, I. (2015). Size does matter: Importance of large bubbles and small-scale hot spots for methane transport. *Environmental Science and Technology*, *49*(3), 1268–1276. https://doi.org/10.1021/es5054286

Delwiche, K., Senft-Grupp, S., & Hemond, H. (2015). A novel optical sensor designed to measure methane bubble sizes in situ. *Limnology and Oceanography: Methods*, *13*(12), 712–721. https://doi.org/10.1002/lom3.10060

Duc, N. T., Crill, P., & Bastviken, D. (2010). Implications of temperature and sediment characteristics on methane formation and oxidation in lake sediments. *Biogeochemistry*, *100*(1–3), 185–196. https://doi.org/10.1007/s10533-010-9415-8

Fonseca, L., Mayer, L., Orange, D., & Driscoll, N. (2002). The high-frequency backscattering angular response of gassy sediments: Model/data comparison from the Eel River Margin, California. *Journal of the Acoustical Society of America*, *111*(6), 2621–2631. https://doi.org/10.1121/1.1471911

Gonzalez-Valencia, R., Magana-Rodriguez, F., Gerardo-Nieto, O., Sepulveda-Jauregui, A., Martinez-Cruz, K., Walter Anthony, K., et al. (2014). In situ measurement of dissolved methane and carbon dioxide in freshwater ecosystems by off-Axis integrated cavity output spectroscopy. *Environmental Science and Technology*, *48*(19), 11421–11428. https://doi.org/10.1021/es500987j

Grasset, C., Mendonça, R., Saucedo, G., Bastviken, D., Roland, F., & Sobek, S. (2018). Large but variable methane production in anoxic freshwater sediment upon addition of allochthonous and autochthonous organic matter: Methanogenic potential of different OC types. *Limnology & Oceanography*, *63*(4), 1488–1501. https://doi.org/10.1002/lno.10786

Grinham, A., Dunbabin, M., Gale, D., & Udy, J. (2011). Quantification of ebullitive and diffusive methane release to atmosphere from a water storage. *Atmospheric Environment*, *45*(39), 7166–7173. https://doi.org/10.1016/j.atmosenv.2011.09.011

Huang, Z., Siwabessy, J., Cheng, H., & Nichol, S. (2018). Using multibeam backscatter data to investigate sediment-acoustic relationships. *Journal of Geophysical Research: Oceans*, *123*(7), 4649–4665. https://doi.org/10.1029/2017JC013638

Itoh, M., Kojima, H., Ho, P.-C., Chang, C.-W., Chen, T.-Y., Hsiao, S. S.-Y., et al. (2017). Integrating isotopic, microbial, and modeling approaches to understand methane dynamics in a frequently disturbed deep reservoir in Taiwan. *Ecological Research*, *32*(6), 861–871. https://doi.org/10.1007/s11284-017-1502-z

Katsnelson, B., Katsman, R., Lunkov, A., & Ostrovsky, I. (2017). Acoustical methodology for determination of gas content in aquatic sediments, with application to Lake Kinneret, Israel, as a case study. *Limnology and Oceanography: Methods*, *15*(6), 531–541. https://doi.org/10.1002/lom3.10178

Katsnelson, B., Uzhansky, E., Lunkov, A., & Ostrovsky, I. (2022). Characterization of the gassy sediment layer in shallow water using an acoustical method: Lake Kinneret as a case study. *Limnology and Oceanography: Methods*, *20*(9), 581–593. https://doi.org/10.1002/lom3.10506

Langenegger, T., Vachon, D., Donis, D., & McGinnis, D. F. (2019). What the bubble knows: Lake methane dynamics revealed by sediment gas bubble composition. *Limnology & Oceanography*, *64*(4), 1526–1544. https://doi.org/10.1002/lno.11133

Langenegger, T., Vachon, D., Donis, D., & McGinnis, D. F. (2022). Methane oxidation dynamics in a stratified lake: Insights revealed from a mass balance and carbon stable isotopes. *Limnology & Oceanography*, *67*(10), 2157–2173. https://doi.org/10.1002/lno.12195

León-Palmero, E., Morales-Baquero, R., & Reche, I. (2020). Greenhouse gas fluxes from reservoirs determined by watershed lithology, morphometry, and anthropogenic pressure. *Environmental Research Letters*, *15*(4), 044012. https://doi.org/10.1088/1748-9326/ab7467

Linkhorst, A., Hiller, C., DelSontro, T., M. Azevedo, G., Barros, N., Mendonça, R., & Sobek, S. (2020). Comparing methane ebullition variability across space and time in a Brazilian reservoir. *Limnology & Oceanography*, *65*(7), 1623–1634. https://doi.org/10.1002/lno.11410

Liu, L., De Kock, T., Wilkinson, J., Cnudde, V., Xiao, S., Buchmann, C., et al. (2018). Methane bubble growth and migration in aquatic sediments observed by X-ray μCT. *Environmental Science and Technology*, *52*(4), 2007–2015. https://doi.org/10.1021/acs.est.7b06061

Liu, L., Sotiri, K., Dück, Y., Hilgert, S., Ostrovsky, I., Uzhansky, E., et al. (2020). The control of sediment gas accumulation on spatial distribution of ebullition in Lake Kinneret. *Geo-Marine Letters*, *40*(4), 453–466. https://doi.org/10.1007/s00367-019-00612-z

Liu, L., Wilkinson, J., Koca, K., Buchmann, C., & Lorke, A. (2016). The role of sediment structure in gas bubble storage and release. *Journal of Geophysical Research: Biogeosciences*, *121*(7), 1992–2005. https://doi.org/10.1002/2016JG003456

Lyons, A. P., Duncan, M. E., Anderson, A. L., & Hawkins, J. A. (1996). Predictions of the acoustic scattering response of free-methane bubbles in muddy sediments. *Journal of the Acoustical Society of America*, *99*(1), 163–172. https://doi.org/10.1121/1.414500

Maeck, A., Hofmann, H., & Lorke, A. (2014). Pumping methane out of aquatic sediments – Ebullition forcing mechanisms in an impounded river. *Biogeosciences*, *11*, 2925–2938. https://doi.org/10.5194/bg-11-2925-2014

Marcon, L., Schwarz, M., Backes, L., Offermann, M., Schreiber, F., Hilgert, S., et al. (2023). Linking sediment gas storage to the methane dynamics in a shallow freshwater reservoir. *Journal of Geophysical Research: Biogeosciences*, *128*(10), e2022JG007365. https://doi.org/10.1029/2022JG007365

Marcon, L., Sotiri, K., Bleninger, T., Lorke, A., Männich, M., & Hilgert, S. (2022). Acoustic mapping of gas stored in sediments of shallow aquatic systems linked to methane production and ebullition patterns. *Frontiers in Environmental Science*, *10*. https://doi.org/10.3389/fenvs.2022.876540

Martinez, D., & Anderson, M. A. (2013). Methane production and ebullition in a shallow, artificially aerated, eutrophic temperate lake (Lake Elsinore, CA). *Science of the Total Environment*, *454–455*, 457–465. https://doi.org/10.1016/j.scitotenv.2013.03.040

Moras, S., Zellmer, U. R., Hiltunen, E., Grasset, C., & Sobek, S. (2024). Predicting methane formation rates of freshwater sediments in different biogeographic regions. *JGR Biogeosciences*, *129*(1), e2023JG007463. https://doi.org/10.1029/2023JG007463

Mudroch, A., & MacKnight, S. D. (1994). Bottom sediment sampling. In *Handbook of techniques for aquatic sediments sampling* (Vol. 2, pp. 29–95).

Natchimuthu, S., Sundgren, I., Gålfalk, M., Klemedtsson, L., Crill, P., Danielsson, Å., & Bastviken, D. (2016). Spatio-temporal variability of lake CH_4 fluxes and its influence on annual whole lake emission estimates. *Limnology & Oceanography*, *61*(S1), S13–S26. https://doi.org/10.1002/lno.10222

Nürnberg, G. K. (2004). Quantified hypoxia and anoxia in lakes and reservoirs. *The Scientific World Journal*, *4*, 42–54. https://doi.org/10.1100/tsw.2004.5

Podgrajsek, E., Sahlée, E., & Rutgersson, A. (2014). Diurnal cycle of lake methane flux. *Journal of Geophysical Research: Biogeosciences*, *119*(3), 236–248. https://doi.org/10.1002/2013JG002327

Rodríguez-Velasco, E., Peralta-Maraver, I., Martínez-García, A., García-Alguacil, M., Picazo, F., Gonçalves, R. J., et al. (2024). Idiosyncratic phenology of greenhouse gas emissions in a Mediterranean reservoir. *Limnology and Oceanography Letters*, *9*(2024), 364–375. https://doi.org/10.1002/lol2.10409

Saunois, M., Stavert, A. R., Poulter, B., Bousquet, P., Canadell, J. G., Jackson, R. B., et al. (2020). The global methane budget 2000–2017. *Earth System Science Data*, *12*(3), 1561–1623. https://doi.org/10.5194/essd-12-1561-2020

Scandella, B. P., Varadharajan, C., Hemond, H. F., Ruppel, C., & Juanes, R. (2011). A conduit dilation model of methane venting from lake sediments. *Geophysical Research Letters*, *38*(6). https://doi.org/10.1029/2011GL046768

Schneider von Deimling, J., Weinrebe, W., Tóth, Z., Fossing, H., Endler, R., Rehder, G., & Spieß, V. (2013). A low frequency multibeam assessment: Spatial mapping of shallow gas by enhanced penetration and angular response anomaly. *Marine and Petroleum Geology*, *44*, 217–222. https://doi.org/10.1016/j.marpetgeo.2013.02.013

Sternlicht, D. D., & de Moustier, C. P. (2003). Time-dependent seafloor acoustic backscatter (10–100 kHz). *Journal of the Acoustical Society of America*, *114*(5), 2709–2725. https://doi.org/10.1121/1.1608018

Tegowski, J., Klusek, Z., & Jakacki, J. (2006). Nonlinear acoustical methods in the detection of gassy sediments. In A. Caiti, N. R. Chapman, J.-P. Hermand, & S. M. Jesus (Eds.), *Acoustic sensing techniques for the shallow water environment: Inversion methods and experiments* (pp. 125–136). Springer. https://doi.org/10.1007/978-1-4020-4386-4_10

Tóth, Z., Spiess, V., & Keil, H. (2015). Frequency dependence in seismoacoustic imaging of shallow free gas due to gas bubble resonance. *Journal of Geophysical Research: Solid Earth*, *120*(12), 8056–8072. https://doi.org/10.1002/2015JB012523

Uzhansky, E., Katsnelson, B., Lunkov, A., & Ostrovsky, I. (2020). Spatial and temporal variability of free gas content in shallow sediments: Lake Kinneret as a case study. *Geo-Marine Letters*, *40*(4), 491–505. https://doi.org/10.1007/s00367-019-00629-4

van Kessel, T., & van Kesteren, W. G. M. (2002). Gas production and transport in artificial sludge depots. *Waste Management*, *22*(1), 19–28. https://doi.org/10.1016/S0956-053X(01)00021-6

Varadharajan, C., & Hemond, H. F. (2012). Time-series analysis of high-resolution ebullition fluxes from a stratified, freshwater lake. *Journal of Geophysical Research*, *117*(G2). https://doi.org/10.1029/2011JG001866

West, W. E., Creamer, K. P., & Jones, S. E. (2016). Productivity and depth regulate lake contributions to atmospheric methane. *Limnology & Oceanography*, *61*(S1), S51–S61. https://doi.org/10.1002/lno.10247

Wik, M., Crill, P. M., Varner, R. K., & Bastviken, D. (2013). Multiyear measurements of ebullitive methane flux from three subarctic lakes. *Journal of Geophysical Research: Biogeosciences*, *118*(3), 1307–1321. https://doi.org/10.1002/jgrg.20103

Wik, M., Thornton, B. F., Bastviken, D., Uhlbäck, J., & Crill, P. M. (2016). Biased sampling of methane release from northern lakes: A problem for extrapolation. *Geophysical Research Letters*, *43*(3), 1256–1262. https://doi.org/10.1002/2015GL066501

Wik, M., Varner, R. K., Anthony, K. W., MacIntyre, S., & Bastviken, D. (2016). Climate-sensitive northern lakes and ponds are critical components of methane release. *Nature Geoscience*, *9*(2), 99–105. https://doi.org/10.1038/ngeo2578

Wildman, R. A., Jr., & Huettel, M. (2012). Acoustic detection of gas bubbles in saturated sands at high spatial and temporal resolution. *Limnology and Oceanography: Methods*, *10*(3), 129–141. https://doi.org/10.4319/lom.2012.10.129

Wilkens, R. H., & Richardson, M. D. (1998). The influence of gas bubbles on sediment acoustic properties: In situ, laboratory, and theoretical results from Eckernförde Bay, Baltic sea. *Continental Shelf Research*, *18*(14–15), 1859–1892. https://doi.org/10.1016/S0278-4343(98)00061-2

Zheng, G., Huang, Y., & Hua, J. (2017). Sound speed, attenuation, and reflection in gassy sediments. *Journal of the Acoustical Society of America*, *142*(2), 530–539. https://doi.org/10.1121/1.4996440

References From the Supporting Information

Bastviken, D. (2009). Methane. In G. E. Likens (Ed.), *Encyclopedia of inland waters* (pp. 783–805). Academic Press. https://doi.org/10.1016/B978-012370626-3.00117-4

Le Mer, J., & Roger, P. (2001). Production, oxidation, emission and consumption of methane by soils: A review. *European Journal of Soil Biology*, *37*(1), 25–50. https://doi.org/10.1016/S1164-5563(01)01067-6